PROCEEDINGS, 51st Workshop on Geothermal Reservoir Engineering
Stanford University, Stanford, California, February 9-11, 2026
SGP-TR-230

Granite Fracture High-Temperature Laboratory Characterization for Utah FORGE

Wenfeng Li*[1], Luke P. Frash*[1], Uwaila C. Iyare[1], Yerkezhan Madenova[1,2], Bijay KC[1], Zhidi Wu[1], Megan Smith[3], Fan Fei[3], and Kayla Kroll[3]

1. Los Alamos National Laboratory, Los Alamos, NM, 87544; 2. University of Wisconsin – Madison, Madison, WI 53706; 3. Lawrence Livermore National Laboratory, Livermore, CA, 94550

* wli23@lanl.gov; lfrash@lanl.gov

Keywords: Shear Strength, Dilation, Fracture, Permeability, Geochemistry

ABSTRACT

We conducted high-temperature triaxial direct-shear (TDS) experiments to investigate the coupled thermo–hydro–mechanical–chemical (THMC) processes controlling fracture creation, deformation, permeability evolution, and geochemical reactivity under conditions representative of the Utah FORGE enhanced geothermal system (EGS) reservoir. Rock specimens were collected from the FORGE well 16A(78)-32 and tested at confining pressures of 36.1 MPa, pore pressures of 22 MPa, and temperatures up to 210 ± 15 °C. The experiments enabled in-situ fracture creation, permeability measurements, mechanical characterization, and effluent geochemical sampling and analysis. Results show that shear-induced fracturing can increase bulk permeability by several orders of magnitude, although permeability evolution remains highly sensitive to shear displacement, stress cycling, temperature, and chemical reactions. High-temperature tests generate shear fractures with low fracture dilation angles (3°–7°), substantially smaller than those measured in comparable low-temperature experiments, suggesting a strong thermal control on shear fracture deformation behavior. Geochemical observations indicate rapid mineral dissolution following fracture creation and evidence for secondary mineral precipitation. Together, these results provide critical insights on fracture flow behavior, THMC coupling, and reservoir simulation at the FORGE site. This work also provides detailed documentation of experimental methods and data interpretation, supporting the dataset archived in the Geothermal Data Repository (GDR) (Frash et al., 2023).

1. INTRODUCTION

Geothermal is a reliable energy option capable of delivering continuous, renewable power and thermal energy. According to the projections by the U.S. Department of Energy (DOE), technological advances could enable geothermal resources to supply up to 60 GWe of electricity in the United States by 2050 (Augustine et al., 2019). Realizing this potential largely requires successful field deployment of Enhanced Geothermal Systems (EGS) that exploit deep and hot rock formations regardless of availability of natural hydrothermal conditions. In EGS reservoirs, artificial stimulation is required to create or reactivate fracture networks to enable fluid circulation at high rates for economic heat recovery (Brown et al., 2012; Tester et al., 2006). Therefore, it is critical to achieve a sophisticated understanding of how fracture-flow evolves under coupled thermo-hydro-mechanical-chemical (THMC) processes, even though significant progress has been made in recent years (Frash et al., 2024; Dobson et al., 2021; Kneafsey et al., 2021).

Supported by the U.S. DOE, the Frontier Observatory for Research in Geothermal Energy (FORGE) is field-scale laboratory for advancing research on EGS. The goal of the FORGE project is to support the development and validation of innovative technologies needed to create, operate, and monitor EGS reservoirs at conditions relevant to commercial deployment (Moore et al., 2020; 2023). The FORGE site is located near Milford, Utah, along the western margin of the Mineral Mountains. Subsurface development at FORGE includes a highly deviated injection well, 16A(78)-32, what was hydraulically stimulated to generate an engineered fracture network. Another well, 16B(78)-32, was then drilled to intersect the stimulated zone and was used as a production well. This results in an injection–production well doublet that is spaced by ~100 m. The engineered reservoir is at an approximate depth of 2.6 km with in-situ formation temperature at 200 °C (Jones et al., 2024; McLennan et al., 2023; Moore et al., 2020; 2023).

Here, we present laboratory experimental results investigating coupled THMC processes governing the stimulation of fractures and the subsequent fluid flow under the FORGE reservoir temperature and pressure conditions. The experiments were conducted using a Triaxial Direct Shear (TDS) approach. This testing approach features creation of rock fractures under in-situ conditions, while allowing for real-time measurements of intact and fractured permeability, fracture deformations, and effluent samples collections for off-line chemistry analysis. The experimental results provide key insights into the potential of hydraulic shear stimulation to enhance fluid flow and enable quantification of critical fracture properties, including strength, frictional properties, dilation tendencies, and chemical reactivity. These measurements provide critical inputs for field-scale reservoir simulations to predict long-term EGS performance at the FORGE site. A parallel goal of this paper is to provide detailed documentation of the experimental methodology and data interpretation to support the dataset archived in the Geothermal Data Repository (GDR) (Frash et al., 2023).

2. MATERIALS AND METHODS

2.1 ROCK AND INJECTION FLUID

Cylindrical rock specimens of 38.1 mm in both diameter and length were prepared from the samples retrieved from the FORGE well 16A(78)-32. A total of nine specimens were tested (Fig. 1), with their lithologic information and experimental conditions summarized in Table 1. The cores include granite and gneiss, with some specimens exhibiting foliation or pre-existing microcracks. The specimens were

prepared such that the dominant fabric or crack orientation was aligned parallel to the cylindrical axis, enabling the TDS testing system to induce shear fractures along the weak planes. This configuration is representative of field conditions, where pre-existing weak planes in reservoir rocks are expected to be activated during reservoir stimulation. The injected fluid was synthetically prepared in the laboratory to replicate the chemistry of the field injectant water sourced from a nearby golf course. The injectant consisted of a 0.5 mM aqueous solution containing KCl, $CaCl_2 \cdot 2H_2O$, $MgCl_2 \cdot 6H_2O$, Na_2SO_4, and $NaHCO_3$ at concentrations of 3.2, 47.7, 33.5, 53.2, and 0.032 mg/L, respectively, dissolved in deionized water.

Table 1. Rock specimens from the FORGE well 16A(78)-32 and the experimental conditions

Specimens [1]	Measured depths (m)	Density (kg/m^3)	Fracture type [2]	Testing Conditions			
				Confining pressure (MPa)	Pore pressure (MPa)	Temperature (°C)	Measured properties [3]
FS01	3345	2724	in-situ	36.1	22.0	175 ± 10	k, PSS, M-C, b_h, b_d, Ψ, γ, Chemistry
FS02	3345	2648	in-situ	36.1	22.0	23 ± 3	k, PSS, M-C, b_h, b_d, Ψ, γ, Chemistry
FS03	3345	2559	in-situ	36.1	22.0	210 ± 15	k, PSS, M-C, b_d, Ψ, Chemistry
FS04	3339	2821	in-situ	36.1	22.0	190 ± 15	k, PSS, M-C, b_h, b_d, Ψ, γ, Chemistry
FS05	1786	2586	saw-cut	36.1	22.0	180 ± 10	k, M-C, b_h, b_d, Ψ, γ, Chemistry
FS06	1786	2575	saw-cut	36.1	22.0	23 ± 3	k, M-C, b_h, b_d, Ψ, γ, Chemistry
FS07	3345	2627	in-situ	36.1	22.0	180 ± 10	k, PSS, M-C, b_h, b_d, Ψ, γ, Chemistry
FS08	3339	2946	in-situ	36.1	22.0	195 ± 15	k, PSS, M-C, b_h, b_d, Ψ, Chemistry
FS09	3339	2788	in-situ	36.1	22.0	195 ± 15	k, PSS, M-C, b_h, b_d, Ψ, γ, Chemistry
GPT-01 [4]	N/A	2593	saw-cut	27.0 – 47.0	22.0	210 ± 15	Proppant conductivity tests; Experiments ongoing for GPT-02(2); Pending data reduction for GPT-01 and GPT-02(2).
GPT-02(1) [4]	1786 (FS06)	2575	saw-cut	36.1	22.0	210 ± 15	
GPT-02(2) [4]	1786 (FS05)	2586	saw-cut	36.1	22.0	210 ± 15	

1: FS05 and FS06 are granite, whereas the others are gneiss. All core samples were retrieved from the FORGE well 16A(78)-32 and prepared with dimensions of 38.1 mm in diameter and 38.1 mm in length.

2: The term "in-situ" refers to the samples that were fractured using the TDS testing approach under high-pressure high-temperature (HPHT) conditions, whereas "saw-cut" means the samples were cut prior to the TDS testing.

3: "k": intact and fractured bulk permeability; "PSS": peak shear strength that is obtained during first fracturing event; "M-C": residual Mohr-Coulomb properties of the fractured core, including residual cohesion and frictional angle; "b_h": fracture hydraulic aperture measured from the flow and pressure data; "b_d": fracture mechanical aperture measured from the radial displacement sensor; "Ψ": fracture dilation angle during shearing; "γ": fracture compressibility in the normal direction; "Chemistry": anion and cation concentrations in the influent and effluent liquids. Section 2.3 provides a detailed theoretical basis for the calculation methods.

4: These are hydraulic conductivity tests of proppant packs in saw-cut fractures. Test GPT-01 used a Colorado gneiss core and was completed successfully; data reduction and analysis are pending. Tests GPT-02(1) and GPT-02(2) used FORGE cores. GPT-02(1) was terminated prematurely due to sleeve failure and flowline clogging, while GPT-02(2) is currently ongoing.

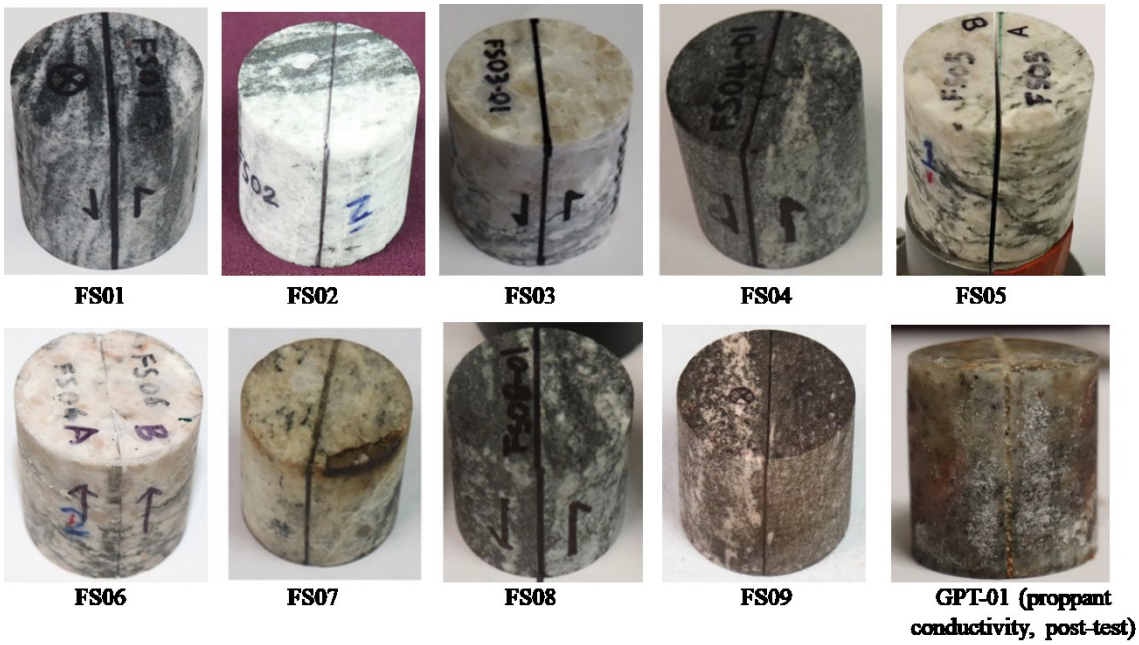

Figure 1: Rock specimens tested using the triaxial-direct shear (TDS) testing system under high-pressure high-temperature conditions. Unlike the others, specimens FS05 and FS06 contain saw-cut fractures prior to the TDS tests.

2.2 THE TRIAXIAL-DIRECT SHEAR (TDS) EXPERIMENTS

The TDS apparatus is a custom-designed experimental system used to create and analyze shear fractures in rock specimens under HPHT conditions. In this system, shear loading is applied through two opposing L-shaped loading platens (Fig. 2a). Controlled axial displacement of the upper platen induces formation of a throughgoing fracture that often aligns parallel to the specimen axis. To enable independent control of the confining and pore pressures, the rock core is wrapped within a sleeve (Fig. 2b) that can isolate the pore fluid and the confining oil at elevated temperatures.

Deformation during shearing is monitored using multiple displacement transducers. Two vertical linear variable differential transformers (LVDTs) measure shear displacement along fracture following its creation, while a third LVDT records lateral deformation associated with fracture opening or closure (Fig. 2d). These sensors provide continuous measurements of mechanical response to changes in pore pressure, confining pressure, and imposed shear displacement. The apparatus also incorporates two fluid ports at each end of the specimen, allowing precise control of pore pressure and monitoring of fluid flow. Direct measurement of pressure gradients across the sample enables robust determination of permeability under various conditions, as demonstrated in previous studies covering various sedimentary and igneous rock types (Li et al., 2021 & 2024; Meng et al., 2022; KC et al., 2024 & 2025a; Iyare et al., 2025).

Unlike room-temperature experiments, high-temperature TDS tests require an improved sample preparation protocol due to material compatibility issues of the heat-shrink sleeve. In particular, heat-shrink teflon sleeves, commonly used in room-temperature TDS experiments, often fail to withstand the pressure differential between the confining oil and pore fluid, especially after fracture formation at temperatures around 200 °C. To prevent sleeve damage following shearing, an additional protective layer of a thick Viton sleeve was installed outside the heat-shrink Teflon sleeve (Fig. 2b,c). Furthermore, metal shims were placed around the specimen periphery at predetermined fracture locations to prevent puncturing of the outer sleeve during and post shear fracturing (Fig. 2b). At elevated temperatures (>200 °C), the half-cylindrical silicone rubber components in contact with the TDS platens (Fig. 2a) were also observed to degrade, potentially clogging the fluid injection and production lines. These material limitations collectively mark the primary challenges preventing TDS testing at temperatures above 200 °C.

Experimental stress, pressure, and temperature conditions were selected to approximate those of the FORGE reservoir based on published field data. Estimates of the maximum and minimum in-situ principal stresses reported in Xing et al. (2020), with magnitudes of 63.4 MPa and 32.5 MPa, respectively, were used to define the laboratory stress state. Although more recent efforts may have refined the in-situ stresses at the FORGE reservoir, the values reported by Xing et al. (2020) were consistently applied across all the TDS experiments to ensure comparability among datasets and minimize variability associated with changing stress conditions between tests. Assuming a potential failure plane inclined at 20° relative to the maximum principal stress, the normal stress acting on the fracture was calculated to be 36.1 MPa and applied as the confining pressure during testing (Iyare et al., 2025). Pore pressure was set to 22 MPa, corresponding to hydrostatic conditions at a depth of approximately 2.2 km. Test temperatures varied slightly throughout the experimental campaign but were chosen to closely represent potential reservoir conditions while remaining within the operational limits of the heating system. In addition, two room-temperature experiments were conducted to isolate the influence of temperature on fracture flow behavior. Details of the testing conditions are summarized in Table 1.

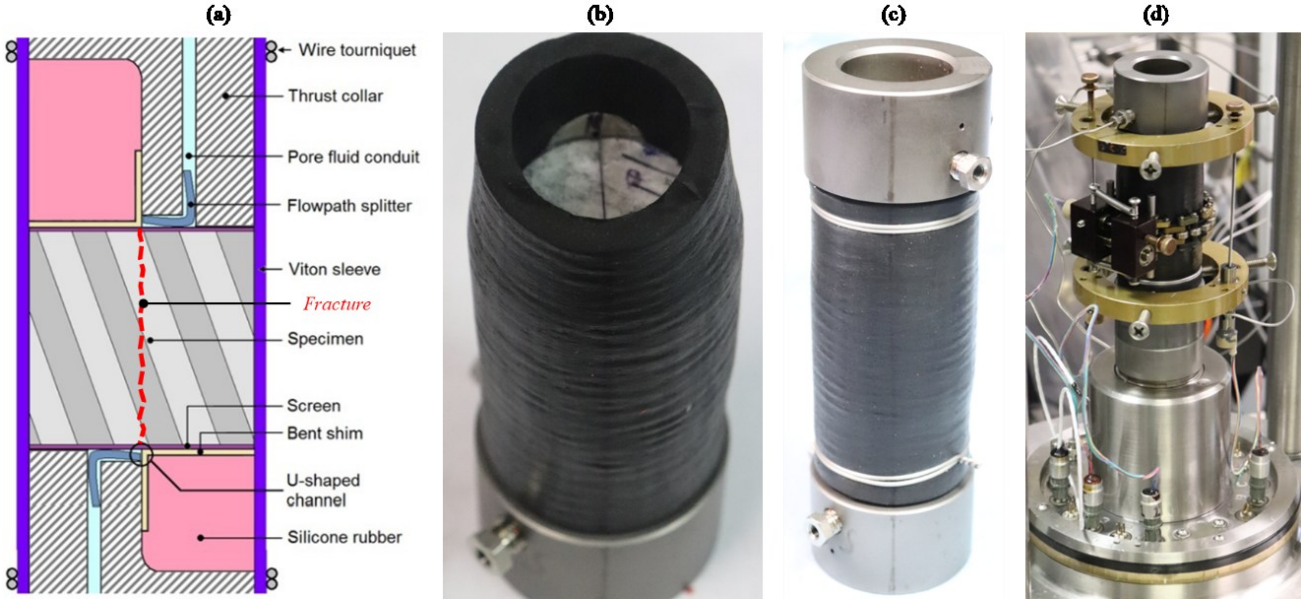

Figure 2: The rock core assembly for the triaxial direct-shear experiments. The specimen is placed between two L-shaped platens so that the weak planes such as foliation is aligned parallel to the shear (vertical) direction for in-situ fracture creation (a). High-temperature viton rubber was used as sleeves to separate the confining and pore pressures control (black rubber in b and c). Two axial LVDTs and one radial LVDT were mounted on the specimen for deformation measurements (d).

The general experimental procedures follow the steps outlined below.

1) *Pre-confinement*: The specimen assembly was placed into the triaxial cell and leak-tested, after which the cell was closed and filled with high-temperature silicone oil.
2) *Heating*: The sample was heated to the target temperature by activating the triaxial cell heater and gradually increasing the cell temperature. A confining pressure of 5 MPa was maintained during heating to prevent steam pressure from inducing unintended fracturing once temperatures exceeded 90 °C.
3) *In-situ confinement*: Confining pressure was increased to the target value of 36.1 MPa, and pore pressure was increased to 22 MPa to establish in-situ reservoir conditions.
4) *Intact rock permeability*: Intact rock permeability was measured under in-situ conditions by injecting fluid into the specimen. Recorded parameters included rock deformation (LVDTs), temperature, injection and production flow rates and pressures, and confining pressure.
5) *Fracturing and flow*: Shear stress was applied to induce fracture formation, with the axial piston displacement rate maintained at approximately 0.002 mm/s throughout all shearing stages. The fracture was displaced incrementally up to 2 mm, during which fracture permeability was measured at multiple shear displacement levels.
6) *Confining stress cycling*: Confining pressure was varied between 24 MPa and 48 MPa at a constant average pore pressure of 22 MPa to evaluate stress-dependent fracture permeability and fracture normal compressibility.
7) *Mohr–Coulomb shear testing*: A constant shear displacement rate was applied along the fracture plane while the confining pressure was adjusted in a stepwise manner to characterize fracture frictional properties. At each confining pressure level, shear stress increased with displacement until reaching a steady value. This procedure provided shear stress as a function of normal stress (equal to confining pressure), enabling determination of Mohr–Coulomb friction parameters under in-situ conditions.
8) *Experiment completion*: Temperature and pressure were gradually reduced to ambient conditions to conclude the experiment.

Key data was continuously logged, including time, temperature, injection pressure, injection rates, production pressure, production rates, confining pressure, and fracture deformation. In addition, effluent samples were collected after each incremental step to directly correlate mechanical deformation and permeability evolution with chemical reactions. Chemical analyses of the effluent samples were conducted using inductively coupled plasma–mass spectrometry (ICP-MS) and inductively coupled plasma–optical emission spectroscopy (ICP-OES). Upon completion of the fracture-flow experiment, a laser scanning system with 5.5-μm horizontal resolution and 0.0001-μm vertical resolution was employed to digitize the 3D surface maps of the fractures, which enables quantification of the fracture roughness according to existing mathematical models, for instance the Joint Roughness Coefficient (JRC) model (Barton 1973; Barton et al., 2023). Together, this integrated approach and data collection minimize uncertainty in characterizing coupled thermal, hydraulic, mechanical, and chemical interactions.

2.3 THEOREY AND DATA ANALYSIS

Darcy's law for single-phase fluid flow was used to calculate the permeability of the rock cores.

$$k = \frac{4Q\mu L}{\pi D^2 (P_i - P_o)} \tag{1}$$

In the above equation, Q is the volumetric flow rate, μ is the dynamic viscosity of water (0.15 cP at 200 °C and 0.9 cP at 23 °C), L is the specimen length, D is the specimen diameter, P_i is the inlet or injection pore pressure, P_o is the outlet or production pore pressure.

Eq. (1) quantifies the bulk permeability of the rock core, regardless of whether a fracture is present. The resulting permeability, k, represents the effective flow capacity averaging to the entire cross-sectional area of the core. This assumption can be misleading for fractured, low-permeability rock cores. As an alternative approach based on the cubic law for flow between parallel plates (Witherspoon et al., 1980), Eq. 2 was used to estimate the fracture hydraulic aperture b_h.

$$b_h = \sqrt[3]{\frac{12\mu LQ}{(P_i - P_o)D}} \tag{2}$$

We emphasize that hydraulic aperture is not equal to the mechanical aperture (b_d) that we have also measured continuously in each experiment using the lateral on-specimen LVDT. A linear correlation, defined by a coefficient N, has been proposed to relate mechanical aperture to hydraulic aperture (Li et al., 2021; Meng et al., 2022; Frash et al., 2024; Iyare et al., 2025), as shown in Eq. (3). This relationship is particularly useful for predicting fracture flow behavior in the field when mechanical aperture is derived from borehole logs prior to circulation testing.

$$b_h = N b_d \tag{3}$$

Subsequent shearing following fracture creation allows measurement of changes in mechanical aperture (Δb_d) as a function of changes in shear displacement ($\Delta\delta$). These data are used to determine the fracture dilation angle (Ψ) during shearing (Eq. 4).

$$\Delta b_d = \Delta\delta \tan\Psi \tag{4}$$

In addition, the experimental data allows us to determine the stress-dependent bulk permeability and fracture hydraulic aperture. Here, effective stress is calculated using the Terzaghi's effective stress theory. For fractured rock cores, the effective normal stress acting on the fracture plane (σ_n') is related to the total normal stress (or the confining pressure, σ_n), the average pore pressure within the fracture ($P_p =$

$\frac{P_i+P_o}{2}$), and the Biot effective stress coefficient (α) through the equation below. For fracture rock cores, it is reasonable to use 1 as the Biot effective stress coefficient (Hu et al., 2010; Li et al., 2022).

$$\sigma_n' = \sigma_n - \alpha P_p \tag{5}$$

Finally, the experimental data also allows us to determine the fracture compressibility by fitting an empirical exponential decay model (Eq. 6) to the measurement data (Li et al., 2021; Iyare et al., 2025).

$$b_d = b_{e0} \cdot e^{-\gamma \sigma_n'} \tag{6}$$

In Eq. (6), the b_d is the measured mechanical aperture, b_{e0} is a fitting parameter representing the mechanical aperture at zero effective normal stress, γ is the fitted fracture compressibility, σ_n' is the effective stress normal to the fracture planes.

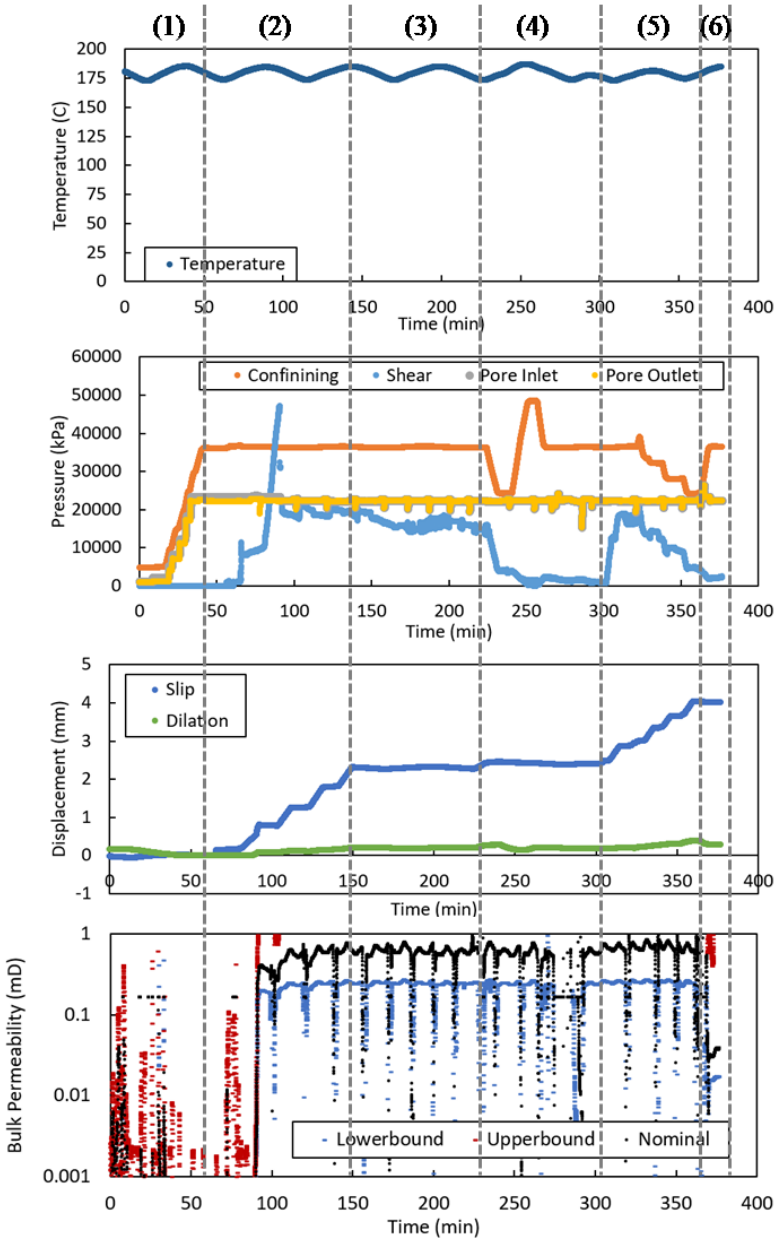

Figure 3: Example testing procedures (FS07) that include: (1) heating, confining and pore pressure loading; (2) fracturing and incremental shear; (3) fluid flow and temporal effluent sampling for chemistry analysis; (4) cyclic confining loading for stress-dependent permeability; (5) Mohr–Coulomb testing for fracture residual shear strength; (6) effluent sampling for chemistry analysis. The time-serial experimental data include temperature, confining pressure, shear stress, inlet and outlet pore pressures and flow rates, fracture shear slip and dilation deformations, and the calculated bulk permeability (Frash et al., 2024).

3. EXAMPLE RESULTS BASED ON THE TEST FS07

In this study, we present results from the TDS experiments conducted on the specimen FS07 to demonstrate the typical experimental procedures and data acquisition. Figure 3 shows the temporal data plots. At the start of the experiment, heating was applied under a pre-confinement stress of 5.0 MPa to prevent steam pressure from fracturing the rock sample at temperatures above 90 °C. Once the system reached the target temperature and pressure conditions, incremental shear displacements were applied to induce fractures. During incremental shearing, the confining stress was held constant to quantify dilation effects. Subsequently, temperature and pressure were maintained constant while permeability measurements were performed and effluent samples were collected for off-line geochemical analysis. Following this, confining stress cycles were conducted to evaluate fracture compressibility and permeability variations as a function of effective normal stress. Thereafter, shear was induced at different confining pressures during the Mohr-Coulomb shear steps to determine residual shear strength. Throughout the test, pore fluid flow was imposed under flow-rate-limited constant-pressure control using two injection pumps and one backpressure pump. Each pump continuously recorded volume, pressure, and flow rate, with pressure measurements redundantly monitored by auxiliary pressure transducers.

The complete dataset for test FS07 was presented in Frash et al. (2024), along with results from several other specimens. For conciseness, we briefly summarize the major findings from test FS07 here. Bulk permeability is shown in the bottom panel of Fig. 3, where fracture formation resulted in an increase in bulk permeability by several orders of magnitude. Figure 4 presents some mechanical testing results. Analysis of the residual Mohr–Coulomb strength yields a cohesion of 2.7 ± 0.5 MPa and a friction angle of 50° ± 5° (Fig. 4, left). The dilation angle was calculated to be 5.3° ± 1.0°, based on a fitted dilation coefficient of 0.09 ± 0.02. Fracture compressibility, using the exponential fit function Eq (6), is estimated as 0.0259 ± 0.01 MPa^{-1} (Fig. 5). Surface profiles in Fig. 6 show the post-shear fracture surfaces of FS07. Notably, FS07 produced relatively little fine gouge material. Additionally, there is clear evidence of slickenside development, including smooth surfaces, white patches, and a waxy texture. We hypothesize that slickensided fracture is resulted from the combined effects of friction, chemical reactions, and elevated temperature.

Figure 7 presents the time series of geochemical data for the experiment FS07. The results indicate rapid dissolution following the creation of fresh fracture surfaces under in situ conditions, followed by a gradual decline in dissolution rates as fluid flow continues. In contrast, magnesium (Mg) and iron (Fe) exhibit behavior that deviates from this general trend. Magnesium originates from the influent fluid, whereas iron concentrations are attributed to corrosion of the steel platens and mesh wires. Under field conditions, analogous sources are expected, with well casing contributing iron and injected fluids supplying magnesium.

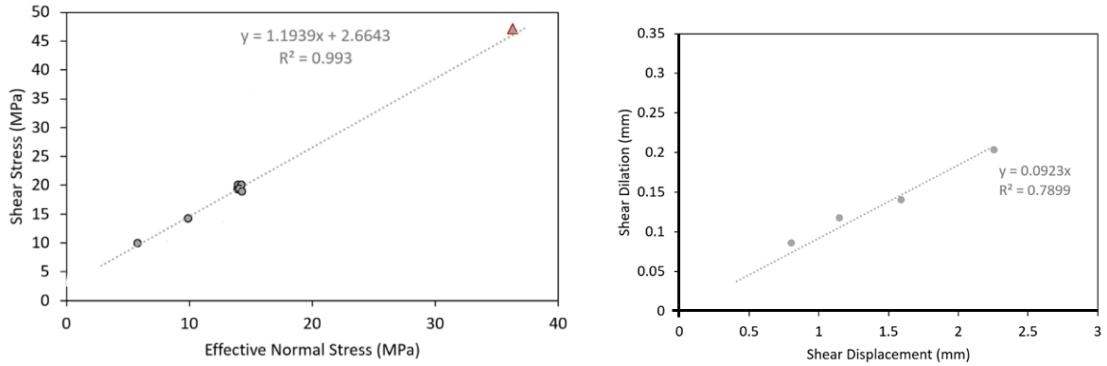

Figure 4: The triaxial direct-shear test enables estimation of the residual Mohr–Coulomb strength (left) and quantification of fracture dilational behavior (right). Residual strength analysis indicates a cohesion of 2.7 ± 0.5 MPa and a friction angle of 50° ± 5°, with a dilation angle of 5.3° ± 1.0° derived from a dilation coefficient of 0.09 ± 0.02 (Frash et al., 2024).

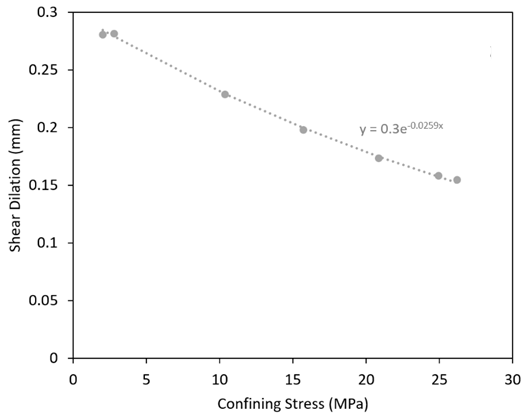

Figure 5: Fracture compressibility from test FS07 is computed as 0.0259 ± 0.01 MPa^{-1} (Frash et al., 2024).

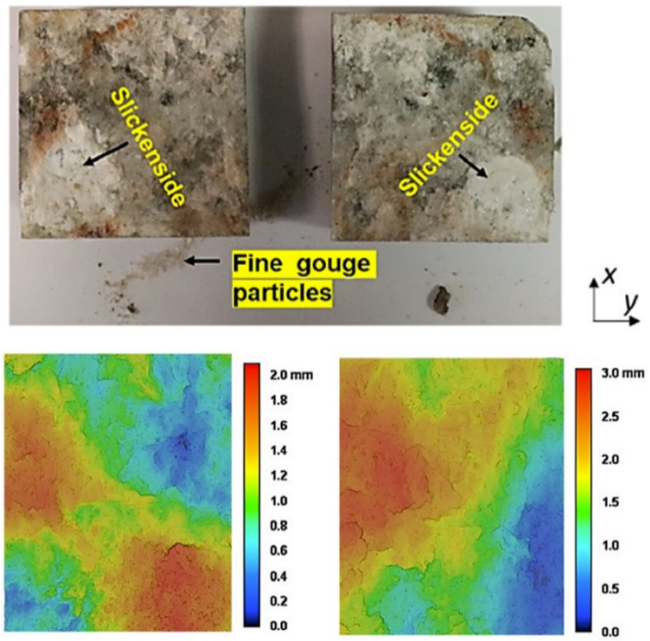

Figure 6: Shear fracture surfaces of specimen FS07 after testing show surface degradation and gouge material. The corresponding digital surface profiles (bottom) are shown in a book-fold configuration, such that the opposing surfaces form approximate mirror images with coincident internal boundaries when aligned (Iyare et al., 2025).

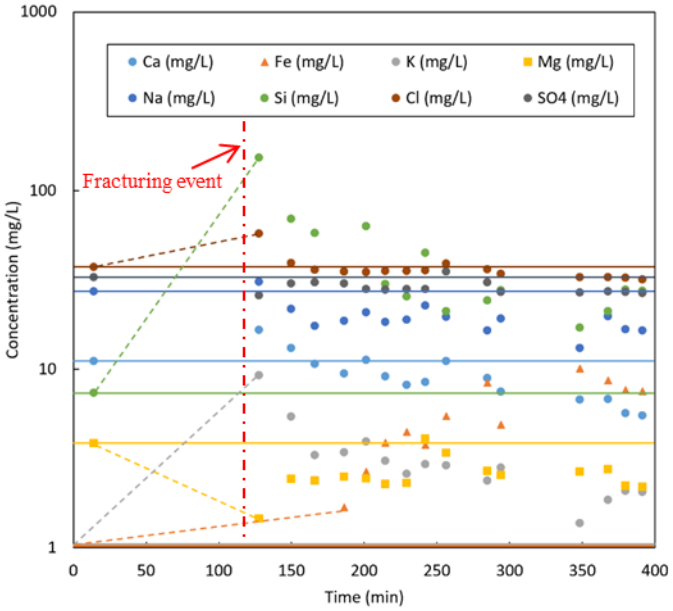

Figure 7: Temporal evolution of major cation and anion concentrations in the effluent. The horizontal reference lines indicating the influent chemistry. Following fracture creation, significant increases in dissolved species reflect rapid dissolution of feldspar (e.g., $KAlSi_3O_8$) and halite (NaCl). Declining magnesium (Mg) concentrations imply mineral precipitation, potentially occurring within the fracture. The slow increase of iron (Fe) can be attributed to the corrosion of the steel platens and mesh screens (Frash et al., 2024).

4. KEY OBSERVATIONS AND DISCUSSIONS

Combining all test results and our previous interpretations (Frash et al., 2024; Iyare et al., 2025; KC et al., 2025b), we summarize the major findings from the experimental campaign.

1. A series of HPHT TDS tests was successfully completed at temperatures up to 210 ± 15 °C. Prior to this campaign, comparable experiments were limited to temperatures ≤ 80 °C (Menefee et al., 2020). The high-temperature testing provided valuable

insights into the selection of suitable materials and the implementation of safe operating procedures. This effort represents a significant advancement in laboratory capabilities for THMC coreflooding experiments under representative in-situ EGS reservoir conditions.

2. Although the measured permeability of intact FORGE rocks is generally very low (< 0.1 μD), pre-existing natural fractures can substantially enhance permeability even without artificial fracturing stimulation. For example, the bulk permeability of specimen FS02, before artificial fracturing, was measured to be approximately 0.1 mD due to the presence of pre-existing microcracks. These observations suggest that highly conductive natural fractures are likely present at the FORGE site.

3. Shear fracturing can increase bulk permeability by several orders of magnitude. For specimens FS03, FS07, and FS09, intact bulk permeability values initially below 0.1 μD increased by approximately three orders of magnitude after fracturing, reaching values greater than 1.0 mD. In specimen FS09, permeability increased by up to five orders of magnitude following the fracturing event. In addition, continued shear displacement along fracture planes generally resulted in further permeability enhancement, by as much as a factor of six. Exceptions, however, do exist in the FS04 where permeability decreased with additional shear displacement. In addition, bulk permeability in fractured cores shows substantial temporal variability, reflecting the combined influences of chemical, mechanical, and thermal processes.

4. Influent and effluent samples were collected to quantify changes in fluid chemistry and to interpret mineral dissolution and precipitation. Complete aqueous geochemical analyses are currently available for test FS07, while analyses for the remaining experiments are still in progress. In FS07, concentrations of SiO_2, Cl, Ca, K, and Na increased rapidly following fracture creation, suggesting enhanced reaction kinetics associated with the exposure of fresh, non-passivated fracture surfaces. These trends suggest dissolution of K-feldspar ($KAlSi_3O_8$) or muscovite ($KAl_2(Si_3Al)O_{10}(OH)_2$), as well as halite (NaCl). In contrast, the inverse trends observed for Mg and SO_4 relative to Si imply magnesite mineral precipitation.

5. Hydroshearing is not always a reliable mechanism for enhancing permeability at the FORGE site. Effective hydroshearing requires three conditions: (a) pre-existing fractures favorably oriented for shear, (b) sufficient in-situ shear stress resulting from stress anisotropy, and (c) pore-pressure buildup enabled by the initial permeability of those fractures. Our experiments show that not all pre-existing fractures in FORGE rock cores are initially permeable for hydroshearing. Moreover, even when hydroshearing is successfully induced, additional shear displacement does not necessarily increase permeability; for example, specimen FS04 exhibited a decrease in bulk permeability with continued shear. In contrast, the formation of fresh shear fractures consistently produced substantial permeability enhancement, often by several orders of magnitude.

6. The high-temperature TDS experiments on FORGE rock cores demonstrate low dilation angles in the range of 3°–7°, which are substantially smaller than those reported for low-temperature TDS tests, where dilation angles reach up to 38° (Meng et al., 2022). Both the high- and low-temperature experiments followed similar testing procedures and data analysis methods. Although different rock types were used in the low-temperature studies (Meng et al., 2022), these lithological differences alone are unlikely to fully account for the large discrepancy in measured dilation angles. We therefore hypothesize that elevated temperature plays a significant role in fracture development, leading to shear behavior characterized by low dilation angles.

7. The FORGE reservoir rocks are characterized by small fracture compressibility, < 0.04 MPa^{-1}, which may help constrain the impact of cyclic normal stress loading on the fracture permeability. As comparison, fracture compressibility has been measured up to 0.069 MPa^{-1} for shales (Tan et al., 2017) and 0.145 MPa^{-1} for schist, amphibolite, and rhyolite (Meng et al., 2022).

8. We emphasize that our tests indicate in-situ shear is likely to produce smooth-planar shear surfaces with small dilation angles, similar to slickensides, based on observation of the post-test fracture planes and the digital fracture surface profilometry scan. Specimens FS07 and FS09 are two typical examples. The slickensided fractures are expected to reduce the benefit of shear fracture stimulation.

All TDS measurement results are publicly available on GDR (Frash et al., 2023), except for a subset of influent and effluent geochemical data that are still under analysis. Hydraulic conductivity tests of proppant packs in saw-cut fractures (Table 1) are either ongoing or pending data reduction and are therefore not included here. All remaining datasets will be deposited in GDR upon completion. These comprehensive datasets provide critical inputs for improving physics-based models, reducing predictive uncertainty, and advancing EGS reservoir stimulation design and management strategies. Specifically, the experiments produce key parameters with well-defined uncertainties that can constrain simulation inputs in THMC simulators incorporating fully coupled 3D earthquake modeling, referred to as “THMC+E” models. This modeling capability accounts for complexities associated with slip-induced gouge formation and reactions, permeability evolution, and induced seismicity, thereby improving EGS design and operational decision-making. Recently, we demonstrated a “THM+E” modeling workflow by simulating stimulation activities at the Utah FORGE site, which significantly improved understanding of fracture generation and reactivation during reservoir stimulation (Fei et al., 2026).

5. CONCLUSIONS

We conducted a campaign of triaxial direct-shear (TDS) experiments using the FORGE rocks under reservoir representative temperature and pressure conditions. These tests enabled controlled in-situ fracture creation and simultaneous measurement of hydraulic, mechanical, and chemical responses. Results demonstrate that shear-induced fracturing can enhance bulk permeability by several orders of magnitude, even in initially low-permeability crystalline rocks. However, permeability evolution is not monotonic and shows strong sensitivity to shear displacement, stress cycling, and time-dependent THMC interactions. In some cases, continued shearing led to reduced permeability,

highlighting the limitations of hydroshearing as a reliable mechanism for flow enhancement. In contrast, the formation of fresh shear fractures consistently resulted in substantial permeability increases.

Another key finding is that high-temperature conditions create fractures with very low dilation angles (3°–7°), significantly smaller than those reported for low-temperature TDS experiments. This suggests that elevated temperature plays a significant role in fracture deformation and subsequent flow behavior by promoting smooth, planar shear surfaces with limited dilation. Such behavior may constrain the long-term effectiveness of hydroshearing stimulation. Geochemical analyses reveal rapid dissolution immediately following fracture creation, followed by declining reaction rates and evidence for secondary mineral precipitation. These observations highlight the importance of chemical processes in governing long-term fracture-flow behavior. Overall, the integrated THMC dataset generated in this study provides critical insights for improving physics-based models and reducing uncertainty in reservoir simulations at FORGE. Most of the dataset is archived in the Geothermal Data Repository (GDR) (Frash et al., 2023) and will be continuously supplemented as the remaining geochemical analyses are completed.

ACKNOWLEDGEMENTS

The authors gratefully acknowledge financial support for this work from the U.S. Department of Energy (DOE) Office of Basic Energy Sciences under FWP LANLE3W1, and from the Geothermal Technologies Office (GTO) Frontier Observatory for Research in Geothermal Energy (FORGE) through grant DE-EE0007080 led by Lawrence Livermore National Laboratory.

REFERENCES

Augustine, C. R., Ho, J. L., & Blair, N. J. GeoVision analysis supporting task force report: Electric sector potential to penetration. *National Renewable Energy Laboratory, NREL/TP-6A20-71833,* (2019).

Barton, N. Review of a new shear-strength criterion for rock joints. *Engineering geology*, *7*(4), pp.287-332. (1973)

Barton, N., Wang, C. and Yong, R. Advances in joint roughness coefficient (JRC) and its engineering applications. *Journal of Rock Mechanics and Geotechnical Engineering*, *15*(12), pp.3352-3379. (2023)

Brown, D. W., Duchane, D. V., Heiken, G., & Hriscu, V. T. Mining the earth's heat: hot dry rock geothermal energy. *Springer Science & Business Media.* (2012).

Dobson, P. F., Kneafsey, T. J., Nakagawa, S., Sonnenthal, E. L., Voltolini, M., Smith, J. T., & Borglin, S. E. Fracture sustainability in Enhanced Geothermal Systems: Experimental and modeling constraints. *Journal of Energy Resources Technology*, *143*,10, 100901, (2021).

Fei, F., Kroll, K., Wang, C., Cusini, M., Smith, M., Burghardt J., Frash, L., Marone, C., and Affinito R. Numerical Study of Hydraulic Stimulations at the Utah-FORGE Geothermal Site with Coupled THM+E Simulations. In *Proceedings of the 51st Workshop on Geothermal Reservoir Engineering*. *Stanford University*. *Stanford, CA* (2026)

Frash, L. P., Iyare, U. C., KC, B., Meng, M., Smith, M., & Kroll, K. High Temperature Triaxial Direct-Shear Testing for FORGE and Field Scale Implications. In *ARMA US Rock Mechanics/Geomechanics Symposium, Golden, CO.* (p. D042S059R005), (2024).

Frash, L.P., Iyare, U., K C, B., Meng, M. Utah FORGE: Triaxial Direct Shear Results. *Geothermal Data Repository*: doi/10.15121/1998752, (2023).

Hu, D.W., Zhou, H., Zhang, F. and Shao, J.F. Evolution of poroelastic properties and permeability in damaged sandstone. *International Journal of Rock Mechanics and Mining Sciences*, *47*(6), pp.962-973. (2010)

Iyare, U.C., Frash, L.P., KC, B., Meng, M., Li, W., Madenova, Y., Peterson, S.K., Gross, M.R., Smith, M.M. and Kroll, K.A. Experimental investigation of shear in granite fractures at Utah FORGE: Implications for EGS reservoir stimulation. *Geothermics*, 131, p.103344. (2025)

Jones, C., Simmons, S., & Moore, J. Geology of the Utah Frontier Observatory for Research in Geothermal Energy (FORGE) Enhanced Geothermal System (EGS) Site. *Geothermics*, *122*, 103054, (2024).

KC, B., Frash, L.P., Mantelli, I.D., Li, W., Purswani, P., Neil, C.W., Meng, M., Germann, T. and Gross, M.R. Laboratory evaluation of cyclic underground hydrogen storage in the temblor sandstone of the San Joaquin Basin, California. *Journal of Energy Storage*, 129, p.117280. (2025a)

KC, B., Frash, L.P., Iyare, U.C., Li, W., Madenova, Y., Smith, M. and Kroll, K., High-Temperature Triaxial Direct Shear Testing for Utah FORGE. In *Proceedings of the 50th Workshop on Geothermal Reservoir Engineering*. *Stanford University*. *Stanford, CA* (2025b)

KC, B., Frash, L.P., Creasy, N.M., Neil, C.W., Purswani, P., Li, W., Meng, M., Iyare, U. and Gross, M.R. Laboratory study of cyclic underground hydrogen storage in porous media with evidence of a dry near-well zone and evaporation induced salt precipitation. *International Journal of Hydrogen Energy*, 71: 515-527. (2024)

Kneafsey, T., Neupane, G., Blankenship, D., Dobson, P., White, M., Morris, J., ... & EGS Collab Team. Scientific Findings to Engineering Realities: Coordination across Collab teams and making the connection to FORGE. *Lawrence Berkeley National Laboratory*. *Report #: LBNL-2001564,* (2021).

Li, W., Frash, L.P., Lei, Z., Carey, J.W., Chau, V.T., Rougier, E., Meng, M., Karra, S., Nguyen, H.T., Rahimi-Aghdam, S. and Bažant, Z.P. Investigating poromechanical causes for hydraulic fracture complexity using a 3D coupled hydro-mechanical model. *Journal of the Mechanics and Physics of Solids*, *169*, p.105062. (2022)

Li, W., Frash, L.P., Welch, N.J., Carey, J.W., Meng, M. and Wigand, M. Stress-dependent fracture permeability measurements and implications for shale gas production. *Fuel*, 290, p.119984. (2021).

Li, W., Neil, C.W., Carey, J.W., Meng, M., Frash, L.P. and Stauffer, P.H. Hydromechanical characterization of gas transport amidst uncertainty for underground nuclear explosion detection. *Journal of Rock Mechanics and Geotechnical Engineering*, 16(6), pp.2019-2032. (2024).

McLennan, J., England, K., Rose, P., Moore, J., & Barker, B. Stimulation of a high-temperature granitic reservoir at the Utah FORGE Site. In *SPE Hydraulic Fracturing Technology Conference and Exhibition, The Woodlands, TX* (p. D031S008R001). SPE. (2023).

Menefee, A.H., Welch, N.J., Frash, L.P., Hicks, W., Carey, J.W., Ellis, B.R. Rapid Mineral Precipitation During Shear Fracturing of Carbonate-Rich Shales. *Journal of Geophysical Research – Solid Earth*, e2019JB018864. (2020)

Meng, M., Frash, L.P., Li, W., Welch, N.J., Carey, J.W., Morris, J., Neupane, G., Ulrich, C. and Kneafsey, T. Hydro-mechanical measurements of sheared crystalline rock fractures with applications for EGS Collab Experiments 1 and 2. *Journal of Geophysical Research: Solid Earth*, 127(2), p.e2021JB023000. (2022)

Moore, J., McLennan, J., Pankow, K., Finnila, A., Dyer, B., Karvounis, D., ... & Damjanac, B. Current activities at the Utah frontier observatory for research in geothermal energy (FORGE): A laboratory for characterizing, creating and sustaining enhanced geothermal systems. In *ARMA US Rock Mechanics/Geomechanics Symposium, Atalanta, GA* (pp. ARMA-2023). ARMA. (2023).

Moore, J., McLennan, J., Pankow, K., Simmons, S., Podgorney, R., Wannamaker, P., ... & Xing, P. The Utah Frontier Observatory for Research in Geothermal Energy (FORGE): A Laboratory for characterizing, creating and sustaining enhanced geothermal systems. In *Proceedings of the 45th Workshop on Geothermal Reservoir Engineering*. *Stanford University*. *Stanford, CA,* (2020).

Tan, Y., Pan, Z., Liu, J., Wu, Y., Haque, A. and Connell, L.D. Experimental study of permeability and its anisotropy for shale fracture supported with proppant. *Journal of Natural Gas Science and Engineering*, *44*, pp.250-264. (2017)

Tester, J. W., Anderson, B. J., Batchelor, A. S., Blackwell, D. D., DiPippo, R., Drake, E. M., ... & Petty, S. The Future of Geothermal Energy. *Massachusetts Institute of Technology,* (2006).

Witherspoon, P. A., Wang, J. S., Iwai, K., & Gale, J. E. Validity of cubic law for fluid flow in a deformable rock fracture. *Water resources research*, *16*(6), 1016-1024, (1980).

Xing, P., McLennan, J., & Moore, J. In-situ Stress Measurements at the Utah Frontier Observatory for Research in Geothermal Energy (FORGE) site. *Energies*, *13*(21), 5842, (2020).